Hindawi Publishing Corporation
EURASIP Journal on Wireless Communications and Networking
Volume 2009, Article ID 195480, 13 pages
doi:10.1155/2009/195480

Research Article

Reduced Complexity Channel Models for IMT-Advanced Evaluation

Yu Zhang,[1] Jianhua Zhang,[1] Peter J. Smith,[2] Mansoor Shafi,[3] and Ping Zhang[4]

[1] *Wireless Technology Innovation Institute, Beijing University of Posts and Telecommunications, P.O. Box 92, Beijing 100876, China*
[2] *Department of Electrical and Computer Engineering, University of Canterbury, Private Bag 4800, 8140 Christchurch, New Zealand*
[3] *Telecom New Zealand, P.O. Box 293, 6001 Wellington, New Zealand*
[4] *Key Laboratory of Universal Wireless Communications, Beijing University of Posts and Telecommunications, P.O. Box 92, Beijing 100876, China*

Correspondence should be addressed to Yu Zhang, yu_zhang@ieee.org

Received 31 July 2008; Revised 6 November 2008; Accepted 26 February 2009

Recommended by Claude Oestges

Accuracy and complexity are two crucial aspects of the applicability of a channel model for wideband multiple input multiple output (MIMO) systems. For small number of antenna element pairs, correlation-based models have lower computational complexity while the geometry-based stochastic models (GBSMs) can provide more accurate modeling of real radio propagation. This paper investigates several potential simplifications of the GBSM to reduce the complexity with minimal impact on accuracy. In addition, we develop a set of broadband metrics which enable a thorough investigation of the differences between the GBSMs and the simplified models. The impact of various random variables which are employed by the original GBSM on the system level simulation are also studied. Both simulation results and a measurement campaign show that complexity can be reduced significantly with a negligible loss of accuracy in the proposed metrics. As an example, in the presented scenarios, the computational time can be reduced by up to 57% while keeping the relative deviation of 5% outage capacity within 5%.

1. Introduction

The pioneering work by Winters [1], Telatar [2], Foschini and Gans [3] ignited enormous interest in multiple input multiple output (MIMO) systems as they have the potential to provide remarkable spectral efficiencies when the channel exhibits rich scattering. Wideband wireless systems with multiple antennas have been recognized as one of the most promising candidates for next generation mobile systems which are also known as IMT-Advanced systems. It is well known that the propagation conditions have a crucial impact on the design, simulation, and deployment of new communication systems. Therefore, it is of great interest to characterize and model the wideband MIMO channel to enable accurate simulations of system performance. Propagation characteristics have been investigated thoroughly based on measured data from channel sounding in various different scenarios [4–8]. An overview of the state-of-the-art channel models is provided in [9]. These channel models can be divided into two major categories: (a) the correlation based models, for example, the Kronecker model [10] and the Weichselberger model [11]; and (b) the parametric or geometry-based stochastic models (GBSMs), for example, the COST 259 directional channel model (DCM) [12], the COST 273 channel model [13], the 3rd Generation Partnership Project (3GPP) spatial channel model (SCM) [14], and the WINNER channel model [15, 16], and so forth. Because of their simplicity, the correlation-based models are widely used for analyzing and designing space-time transmission technologies. The GBSM is more complex and less easy to use. One feature of a GBSM is that the simulation is divided into a number of drops which can be thought as channel segments with infinite time. Within each drop, different random geometries are generated. This

modeling methodology is adopted by the International Telecommunication Union (ITU) for the evaluation of IMT-Advanced systems [17].

In comparison with the broadly adopted traditional tapped delay line (TDL) models in the GSM and IMT-2000 systems, there are two main challenges for the IMT-Advanced channel model. Firstly, the TDL models in [18, 19] have an invariant channel profile. (The "channel profile" stands for the channel characteristics over a fading distance of tens of wavelengths, in spatial, temporal, and frequency domains, including the power delay profile (PDP), power angular spectrum (PAS), Doppler spectrum, and so forth.) However, even for a single link, geometry-based MIMO channel models need multiple channel profiles to accurately characterize the extra degrees of freedom induced by employing multiple antennas. As a result, far more random variables (RVs) have to be embedded into the channel model than are required by the TDL models. Secondly, because of the higher data rates targeted with a system bandwidth of up to 100 MHz, many more multipath components (MPCs) can be resolved, which leads to an increase in the number of taps for wideband MIMO channel models. Since the system level evaluation of radio interface technologies (RITs) usually requires the generation of multiple users dropped into a 19 hexagonal cell network, these two challenges faced by GBSMs make the evaluation a time consuming exercise. Hence, there is an urgent need to simplify the geometry-based MIMO channel models. As the correlation-based models have greatly reduced computational complexity, several papers have tried to bridge the gap between the correlated models and GBSMs. The separability of spatial-temporal correlation in the 3GPP SCM model is investigated in [20], which proposed a correlation-based model to replace the geometry-based model. A numerically efficient approximation of spatial correlation models is proposed in [21], which shows a good fit to the existing parametric models with a uniform linear array (ULA) or uniform circular array (UCA) for an angular spread (AS) smaller than 10°. A simplified approach to apply the 3GPP SCM model was suggested in [22], which was also proposed for the evaluation of the 3GPP long-term evolution (LTE) systems. Correlation-based replacements of the GBSM can substantially reduce the computational complexity. However, in such simplified models the antenna geometries and radiation patterns cannot be altered easily by the user of the model. On the other hand, this feature is automatically enabled by the geometry-based modeling for the propagation parameters and antennas.

In this paper, we investigate five possible simplifications to the GBSM model. These simplifications are much more straightforward than those obtained by converting a GBSM to its correlation-based counterpart. A series of metrics are proposed to evaluate the impact of the simplification on the channel model behavior. These metrics cover various different perspectives of the assessment of RITs with MIMO applications, including spatial multiplexing, spatial diversity, symbol error probability, and temporal behavior. The proposed simplifications and metrics are validated with a baseline model which is extracted from MIMO channel measurements in both indoor and outdoor environments. A computational complexity analysis is also presented. Since the simplifications are made under the original structure of the GBSM, the ability to select values for physically-based geometric parameters is maintained. Hence, the users of the simplified models can control the antenna configurations and link geometries as they do with the GBSM, while experiencing lower computational effort.

The main contributions of this paper are as follows:

(i) a range of broadband metrics are proposed and used for evaluating the full system behavior of wideband MIMO channel models;

(ii) a series of potential simplifications to the IMT-Advanced channel model are developed. The simplified models have fixed and fewer parameters that result in a negligible loss of performance as verified by a range of metrics;

(iii) measurements of an indoor channel with both line-of-sight (LOS) and scattered components were taken in China. The data was used to fit a WINNER style model [17] as the baseline GBSM. The metrics were then used to compare the simplified models with the GBSM and with the measured data;

(iv) the metrics were also evaluated with an outdoor non line-of-sight (NLOS) channel in the WINNER model [16] to demonstrate the validity of proposed simplifications.

The rest of the paper is organized as follows. A GBSM baseline model is briefly described in Section 2. A series of metrics for evaluating the performance of simplified wideband channel models are presented in Section 3. The proposed simplifications are described in Section 4. A comparative analysis of the simulation results and conclusions are given in Sections 5 and 6, respectively.

2. Baseline Channel Model

Currently, the primary channel model [17] for IMT-Advanced system evaluation is based on the WINNER channel model. Hence, in this paper we take the WINNER model as a baseline. Consider a single downlink of a wideband MIMO system with an S-element BS array and a U-element MS array. The channel impulse response (CIR) at time t, delay τ is modeled as

$$\mathbf{H}(\tau,t)=\sqrt{\frac{K}{K+1}}\mathbf{H}_0(t)\delta(\tau)+\sqrt{\frac{1}{K+1}}\sum_{n=1}^{N}\mathbf{H}_n(t)\delta(\tau-\tau_n), \tag{1}$$

where K is the Rician K-factor on a linear scale, $\mathbf{H}_0(t)$ is the channel coefficient matrix corresponding to the LOS ray, N is the number of clusters, $\mathbf{H}_n(t)$, $n=1,2,\ldots,N$, is the nth NLOS channel coefficient component, and $\delta(\cdot)$ is the Dirac delta function. Here, we assume that the clusters are the zero-delay-spread-clusters (ZDSCs) defined in [15], that is, a cluster is constituted by a number of rays, or propagation paths, diffused in angle domains. The rays within the same

cluster have the same propagation delay, and the power dispersion of a cluster in angle domains is characterized by cluster angular spread of departure (ASD) and cluster angular spread of arrival (ASA). The elements of the $U \times S$ matrix $\mathbf{H}_n(t) = (h_{usn}(t))$ are given by

$$h_{us0}(t) = \mathbf{c}_{\mathrm{BS},s}^{\mathrm{T}}(\phi_{\mathrm{LOS}}) \cdot \mathbf{X}(\mathbf{\Phi}_{\mathrm{LOS}}) \cdot \mathbf{c}_{\mathrm{MS},u}(\varphi_{\mathrm{LOS}}) \cdot \exp\left[jk\|\mathbf{v}\| \cos\left(\varphi_{\mathrm{LOS}} - \phi_v\right)t\right] \tag{2}$$

for $n = 0$,

$$h_{usn}(t) = \sqrt{\frac{P_n}{M}} \sum_{m=1}^{M} \mathbf{c}_{\mathrm{BS},s}^{\mathrm{T}}(\phi_{nm}) \cdot \mathbf{X}(\mathbf{\Phi}_{nm}, \kappa_{nm}) \cdot \mathbf{c}_{\mathrm{MS},u}(\varphi_{nm}) \cdot \exp\left[jk\|\mathbf{v}\| \cos\left(\varphi_{nm} - \phi_v\right)t\right] \tag{3}$$

for $n = 1, 2, \ldots, N$. In (2) and (3), $(\cdot)^{\mathrm{T}}$ stands for matrix transposition, P_n is the power resulting from the nth cluster, M is the number of rays in each cluster. The angles in (2) and (3) are illustrated in Figure 1, where ϕ_{LOS} is the angle of departure (AoD) for the LOS ray with respect to the BS broadside, φ_{LOS} is the angle of arrival (AoA) for the LOS ray with respect to the MS broadside, ϕ_{nm} is the AoD for the mth ray of the nth cluster with respect to the BS broadside, while φ_{nm} is the AoA with respect to the MS broadside, the mean AoD and mean AoA of the nth cluster is defined as $\phi_n = (1/M)\sum_{m=1}^{M} \phi_{nm}$ and $\varphi_n = (1/M)\sum_{m=1}^{M} \varphi_{nm}$, respectively. ϕ_v is the angle of the MS velocity vector $\mathbf{v}$ with respect to the MS broadside. $\mathbf{c}_{\mathrm{BS},s}(\phi_{nm}) = [c_{\mathrm{BS},s}^{\mathrm{V}}(\phi_{nm}), c_{\mathrm{BS},s}^{\mathrm{H}}(\phi_{nm})]^{\mathrm{T}}$ is the complex antenna response of the sth element of the BS array in the direction of ϕ_{nm} with respect to the reference phase center of the array, with $c_{\mathrm{BS},s}^{\mathrm{V}}(\cdot)$ and $c_{\mathrm{BS},s}^{\mathrm{H}}(\cdot)$ referring to the vertical and horizontal polarization directions, respectively. The vector $\mathbf{c}_{\mathrm{MS},u}(\varphi_{nm})$ is defined similarly. $\mathbf{\Phi}_{nm} = [\Phi_{nm}^{\mathrm{VV}}, \Phi_{nm}^{\mathrm{VH}}, \Phi_{nm}^{\mathrm{HV}}, \Phi_{nm}^{\mathrm{HH}}]^{\mathrm{T}}$ is the initial random phase vector of the mth ray of the nth cluster. The superscripts used in $\Phi_{nm}^{p_1 p_2}$ denote that the ray originates in the p_1 direction and arrives in the p_2 direction. $\mathbf{\Phi}_{\mathrm{LOS}} = [\Phi_{\mathrm{LOS}}^{\mathrm{VV}}, \Phi_{\mathrm{LOS}}^{\mathrm{HH}}]^{\mathrm{T}}$ is the initial random phase vector for the LOS ray. The polarization matrices $\mathbf{X}(\mathbf{\Phi}_{\mathrm{LOS}})$ and $\mathbf{X}(\mathbf{\Phi}_{nm}, \kappa_{nm})$ are given by

$$\mathbf{X}(\mathbf{\Phi}_{\mathrm{LOS}}) = \begin{pmatrix} \exp\left(j\Phi_{\mathrm{LOS}}^{\mathrm{VV}}\right) & 0 \\ 0 & \exp\left(j\Phi_{\mathrm{LOS}}^{\mathrm{HH}}\right) \end{pmatrix},$$

$$\mathbf{X}(\mathbf{\Phi}_{nm}, \kappa_{nm}) = \begin{pmatrix} \exp\left(j\Phi_{nm}^{\mathrm{VV}}\right) & \sqrt{\kappa_{nm}} \exp\left(j\Phi_{nm}^{\mathrm{VH}}\right) \\ \sqrt{\kappa_{nm}} \exp\left(j\Phi_{nm}^{\mathrm{HV}}\right) & \exp\left(j\Phi_{nm}^{\mathrm{VV}}\right) \end{pmatrix}, \tag{4}$$

where κ_{nm} is the inverse of the XPR for the nth cluster and mth ray. The XPR in decibels, is independent for each cluster and ray, and follows the Gaussian distribution $\mathcal{N}(\mu_{\mathrm{XPR}}, \sigma_{\mathrm{XPR}}^2)$. The constant k is the wave number $2\pi/\lambda$ with λ denoting the carrier wavelength in meters.

For each drop, the parameters required by (2) and (3) can be broken down into three sets: the LOS parameters $\{K, \phi_{\mathrm{LOS}}, \varphi_{\mathrm{LOS}}, \mathbf{\Phi}_{\mathrm{LOS}}\}$, the cluster parameters $\{(P_n, \tau_n, \phi_n, \varphi_n) : n = 1, 2, \ldots, N\}$, and the ray parameters $\{(\phi_{nm}, \varphi_{nm}, \mathbf{\Phi}_{nm}, \kappa_{nm}) : n = 1, 2, \ldots, N; m = 1, 2, \ldots, M\}$. According to the modeling methodology behind the WINNER channel model, for a specific scenario, the root-mean-square (RMS) delay spread (DS) τ_{RMS}, azimuth ASD ϕ_{RMS}, azimuth ASA φ_{RMS}, standard deviation of shadow fading (SF) $\sigma_{\xi,\mathrm{dB}}$, and the Rician K-factor K_{dB} for the LOS case are correlated log-normal RVs. Hence, the 5-dimensional random vector $\mathbf{L} = [\log_{10}(\tau_{\mathrm{RMS}}), \log_{10}(\phi_{\mathrm{RMS}}), \log_{10}(\varphi_{\mathrm{RMS}}), \sigma_{\xi,\mathrm{dB}}, K_{\mathrm{dB}}] \sim \mathcal{N}(\boldsymbol{\mu}_{\mathbf{L}}, \mathbf{\Sigma}_{\mathbf{L}})$, where $\boldsymbol{\mu}_{\mathbf{L}} = [\mu_{\mathrm{DS}}, \mu_{\mathrm{ASD}}, \mu_{\mathrm{ASA}}, 0, \mu_{K,\mathrm{dB}}]$ is the mean vector and $\mathbf{\Sigma}_{\mathbf{L}}$ is the covariance matrix. The standard deviations of the normal RVs in $\mathbf{L}$ are denoted by σ_X, and the cross-correlation coefficients between the normal RVs in $\mathbf{L}$ are denoted by ρ_{XY}, where X and Y are placeholders for DS, ASD, ASA, SF, and K. The detailed definitions of μ_X, σ_X, and ρ_{XY} are summarized in Table 1, where $\mathrm{E}(\cdot)$ is the expectation operator, $\mathrm{Var}(X)$ stands for the variance of RV X, and $\mathrm{Corr}(X, Y)$ denotes the cross-correlation coefficient of two RVs X and Y. The five parameters in $\mathbf{L}$ are called large-scale parameters (LSPs) [16] since they are invariant in a channel segment, or drop, which covers a fading distance of the order of tens of wavelengths.

The realization of the Rician-K factor together with realizations of the other LSPs, that is, the realization of the Gaussian random vector $\mathbf{L}$, are drawn to follow the distribution $\mathcal{N}(\boldsymbol{\mu}_{\mathbf{L}}, \mathbf{\Sigma}_{\mathbf{L}})$. The LOS ray angles, ϕ_{LOS} and φ_{LOS}, are geometrically determined by the relative positions of BS and MS, and by the broadside orientations of both BS and MS array. The cluster parameters, $\{\tau_n\}$, $\{P_n\}$, and $\{(\phi_n, \varphi_n)\}$ are sequentially generated according to the exponential delay distributions, exponential/uniform power delay profile (PDP), and wrapped Gaussian power angular spectrum (PAS), respectively. The shape of delay distributions, PDP and PAS, can be determined by realizations of the LSPs, that is, τ_{RMS}, ϕ_{RMS}, and φ_{RMS}, which are generated together with K as mentioned above. The ray parameters $\{(\phi_{nm}, \varphi_{nm}) : n = 1, 2, \ldots, N; m = 1, 2, \ldots, M\}$ are obtained by adding predefined offset angles to ϕ_n or φ_n to follow Laplacian PASs with given per cluster angular spread. The elements in the initial phases $\mathbf{\Phi}_{\mathrm{LOS}}$ and $\mathbf{\Phi}_{nm}$ are independent and identically distributed uniform in $(-\pi, \pi)$. A detailed procedure of the generation of these parameters can be found in [16]. Within a drop, all these parameters are invariant. Thus, a single drop cannot reflect the propagation characteristics for a given scenario and multiple-drop simulation is needed even for link-level performance evaluation.

3. Evaluation Metrics for Wideband MIMO Channels

To evaluate the impact of various potential simplifications to the channel model, proper metrics for wideband MIMO channels are needed. Usually, spatial-temporal correlations are used as two simple but fundamental metrics for MIMO channel models. However, this paper aims to go further and develops a thorough approach to studying the full system behavior, through a more complex set of metrics. This set includes mutual information, diversity gain, error

Table 1: Definitions of first- and second-order statistics of LSPs.

$\mu_{\mathrm{DS}} = \mathrm{E}[\log_{10}(\tau_{\mathrm{RMS}})]$	$\rho_{\mathrm{ASD,DS}} = \mathrm{Corr}[\log_{10}(\phi_{\mathrm{RMS}}), \log_{10}(\tau_{\mathrm{RMS}})]$
$\mu_{\mathrm{ASD}} = \mathrm{E}[\log_{10}(\phi_{\mathrm{RMS}})]$	$\rho_{\mathrm{ASA,DS}} = \mathrm{Corr}[\log_{10}(\varphi_{\mathrm{RMS}}), \log_{10}(\tau_{\mathrm{RMS}})]$
$\mu_{\mathrm{ASA}} = \mathrm{E}[\log_{10}(\varphi_{\mathrm{RMS}})]$	$\rho_{\mathrm{ASD,SF}} = \mathrm{Corr}[\log_{10}(\phi_{\mathrm{RMS}}), \sigma_{\xi,\mathrm{dB}}]$
$\mu_{K,\mathrm{dB}} = \mathrm{E}[K_{\mathrm{dB}}]$	$\rho_{\mathrm{ASA,SF}} = \mathrm{Corr}[\log_{10}(\varphi_{\mathrm{RMS}}), \sigma_{\xi,\mathrm{dB}}]$
	$\rho_{\mathrm{ASD,ASA}} = \mathrm{Corr}[\log_{10}(\phi_{\mathrm{RMS}}), \log_{10}(\varphi_{\mathrm{RMS}})]$
$\sigma^2_{\mathrm{DS}} = \mathrm{Var}[\log_{10}(\tau_{\mathrm{RMS}})]$	$\rho_{\mathrm{DS,SF}} = \mathrm{Corr}[\log_{10}(\tau_{\mathrm{RMS}}), \sigma_{\xi,\mathrm{dB}}]$
$\sigma^2_{\mathrm{ASD}} = \mathrm{Var}[\log_{10}(\phi_{\mathrm{RMS}})]$	$\rho_{\mathrm{ASD,K}} = \mathrm{Corr}[\log_{10}(\phi_{\mathrm{RMS}}), K_{\mathrm{dB}}]$
$\sigma^2_{\mathrm{ASA}} = \mathrm{Var}[\log_{10}(\varphi_{\mathrm{RMS}})]$	$\rho_{\mathrm{ASA,K}} = \mathrm{Corr}[\log_{10}(\varphi_{\mathrm{RMS}}), K_{\mathrm{dB}}]$
$\sigma^2_{K,\mathrm{dB}} = \mathrm{Var}[K_{\mathrm{dB}}]$	$\rho_{\mathrm{DS,K}} = \mathrm{Corr}[\log_{10}(\tau_{\mathrm{RMS}}), K_{\mathrm{dB}}]$
$\sigma^2_{\mathrm{SF}} = \mathrm{Var}[\sigma_{\xi,\mathrm{dB}}]$	$\rho_{\mathrm{SF,K}} = \mathrm{Corr}[\sigma_{\xi,\mathrm{dB}}, K_{\mathrm{dB}}]$

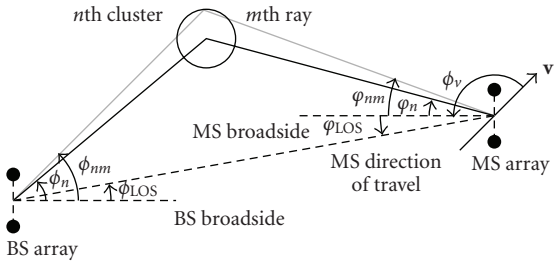

Figure 1: Definition of angles in WINNER channel model.

rate, and temporal behavior. Recall that, in the baseline model, a scenario is characterized by multiple drops with different realizations of LSPs. For either link- or system-level simulation, the overall performance of all drops is concerned. Based on this fact, these metrics are designed for evaluating the average behavior over multiple drops. With such metrics, we can try to examine whether the proposed simplified model has equivalent behavior in the scenario level. The proposed metrics are described in what follows.

3.1. Spatial Multiplexing Metric. Outage capacity is a widely adopted metric to evaluate the spatial multiplexing ability of an MIMO channel, because it is the main benefit provided by this MIMO mode. The outage capacity, or the cumulative distribution function (CDF) of the channel capacity, when the channel is unknown to the transmitter is preferred to the ergodic capacity which can be derived from the CDF. This is because the ergodic capacity is often insensitive to the exact channel characteristics, whereas the capacity distribution is more easily affected. Hence, the outage capacity provides a more rigorous test. The capacity of a time-invariant frequency-selective fading MIMO channel is given by [23]

$$C = \frac{1}{B}\int_B \log_2 \det\left[\mathbf{I}_U + \frac{\rho}{S}\mathbf{H}(f)\mathbf{H}(f)^{\dagger}\right]\mathrm{d}f, \tag{5}$$

where $(\cdot)^{\dagger}$ stands for conjugate transpose, B is the bandwidth, ρ denotes the signal-to-noise ratio (SNR) and $\mathbf{H}(f)$ is the normalized frequency domain channel matrix with unitary average channel power gain, that is,

$$\mathrm{E}\left(\|\mathbf{H}(f)\|_{\mathrm{F}}^2\right) = US. \tag{6}$$

Note that $\mathbf{H}(f)$ is the transform of the composite impulse response with the delays, so the capacity obtained from (5) is the broadband capacity. In (5), we have assumed equal power allocation and no water filling is done both in the frequency and space domains. Given an SNR ρ, the $100q\%$ outage capacity C_q is defined as the spatial multiplexing metric, that is, $\Pr[C < C_q] = q$.

3.2. Spatial Diversity Metric. When the channel is known to the transmitter, spatial diversity is related to the dominant eigenmodes of the channel matrix. Hence, we choose the marginal CDF of each ordered eigenvalue of the channel correlation matrix as the spatial diversity metric. Let $\lambda_{(n)}(f)$, $n = 1, 2, \ldots, U$, be the eigenvalues of $\mathbf{H}(f)\mathbf{H}(f)^{\dagger}$ in descending order, that is,

$$\lambda_{(1)}(f) \geqslant \lambda_{(2)}(f) \geqslant \cdots \geqslant \lambda_{(U)}(f). \tag{7}$$

Note that, (7) implies that $\lambda_{(n)}(f) = 0$ for $r < n \leqslant U$, where $r = \mathrm{rank}[\mathbf{H}(f)\mathbf{H}(f)^{\dagger}]$. For $n = 1, 2, \ldots, r$, the r empirical distribution functions obtained from $\{\lambda_{(n)}(f) : f \in [-B/2, B/2]\}$ are used as the spatial diversity metric. Note that this approach is quite unusual. The eigenvalues are being considered as random variables over frequency rather than over different channel realizations for the same frequency. For example, considering the maximum eigenvalue, a range of values is obtained from measurements or simulations over frequency and not over different channel realizations. This reflects the focus of the paper on broadband metrics.

3.3. Symbol Error Probability. The exact symbol error probability (SER) of singular value decomposition (SVD)-based MIMO receivers using uncoded transmission is derived in [24] for flat-fading channels. We generalize the result to the frequency selectivity case. If only the first m principal eigen modes are activated for the SVD-based transmission and the uncoded BPSK scheme is adopted, the symbol error probability for a given SNR level ρ is given by

$$\mathrm{SER}(\rho) = 1 - \frac{1}{2^m B}\int_{-B/2}^{B/2} \mathrm{E}\left\{\prod_{i=1}^{m} \mathrm{erfc}\left(-\sqrt{\frac{\rho\lambda_{(i)}(f)}{2S}}\right)\right\}\mathrm{d}f, \tag{8}$$

where $\mathrm{erfc}(x)$ is the complementary error function. For a fixed SER value, let the required SNR be ρ_0 for the baseline

model and ρ_1 for the simplified model. The SNR shift, $\Delta\rho = |\rho_1 - \rho_0|$, is defined as the SER metric.

3.4. Temporal Behavior of MIMO Capacity. The capacity of the time-variant MIMO channel is a stochastic process. The temporal behavior of the MIMO channel model can be partially reflected by the level crossing rate (LCR) across a capacity level C_T (denoted as $\mathsf{LCR}(C_T)$) and the average fading duration (ADF) of the capacity process below C_T [25]. Let μ_C be the mean capacity, and σ_C^2 be the capacity variance. Defining the standardized capacity values as $\widetilde{C} = (C - \mu_C)/\sigma_C$, we focus on the $\mathsf{LCR}(\widetilde{C}_T)$ which is the LCR of the normalized capacity, $\widetilde{C}$, across $\widetilde{C}_T$. Results are shown for $\mathsf{LCR}(\widetilde{C}_T)$ normalized by the maximum Doppler frequency f_D, versus the outage probability given by $P_{out}(\widetilde{C}_T) = \Pr[\widetilde{C} < \widetilde{C}_T]$ [25].

4. Potential Simplifications

4.1. Clipping Clusters with Lower Power. In [26], the computational complexity of channel model simulation was divided into three different categories: (a) complexity of channel coefficient generation, (b) number of required parameters, and (c) the complexity of simulation. Both (a) and (c) are proportional to the number of delay taps. Hence, the computational complexity can be reduced if the number of delay taps can be reduced. However, the impact of reducing the number of delay taps needs to be investigated. The clipping is based on the fact that the average power of some clusters is relatively low with respect to the maximum cluster power. Consider a scenario with N clusters, where the average cluster power of the nth cluster is P_n in decibels. Denote the cluster indexing set as $\mathcal{I} = \{1, 2, \ldots, N\}$. For a given cluster power threshold, P_{th} in decibels, the cluster is clipped if its power is below this threshold when the power of the dominant cluster is chosen as a reference. The reduced number of clusters is an RV

$$N_{clipped} = \sum_{n=1}^{N} I\left(P_n < \max_{k\in\mathcal{I}} P_k - P_{th}\right), \tag{9}$$

where $I(A)$ is the indicator function of event A, namely,

$$I(A) = \begin{cases} 1, & \text{event } A \text{ is true,} \\ 0, & \text{otherwise.} \end{cases} \tag{10}$$

As mentioned in [26], the computational time for simulation is dominated by the convolution operation, and the time required by such an operation is proportional to the number of delay taps (or the number of clusters). Consequently, if we normalize the computational time after clipping by the time required before clipping, the *normalized computational time* (NCT) can be defined as the ratio of the average number of remaining clusters to the number of original clusters, that is,

$$\mathsf{NCT}(P_{th}) = 1 - \frac{1}{N}\mathrm{E}(N_{clipped}). \tag{11}$$

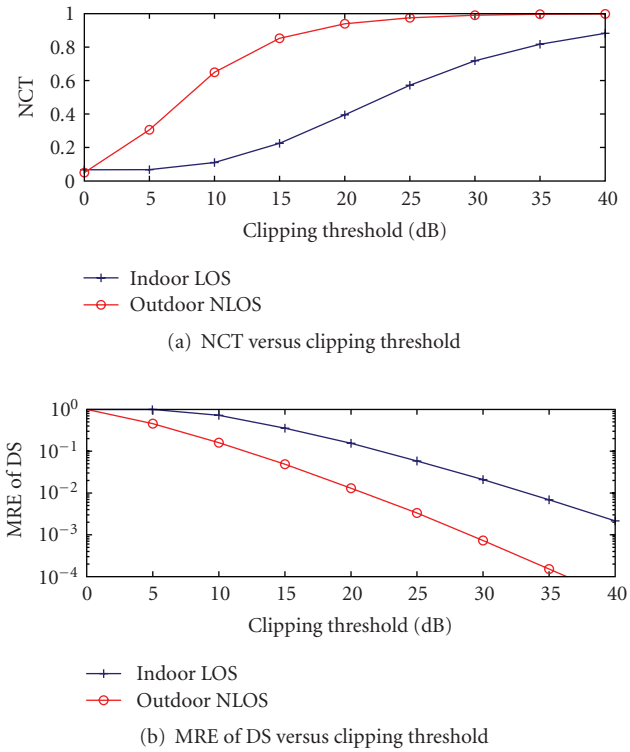

(a) NCT versus clipping threshold

(b) MRE of DS versus clipping threshold

FIGURE 2: The impact of clipping threshold on the efficiency and the accuracy (averaged over 10^4-drop runs).

When the clipping threshold $P_{th} = 0$ dB, only the cluster with maximum power remains. Thus the minimum NCT is obtained, that is, $\mathsf{NCT}(0) = 1/N$. When $P_{th} \to \infty$, no cluster will be clipped and NCT converges to one. The NCT indicates the benefit gained by clipping the low-power clusters. Figure 2(a) shows the relationship of NCT versus the clipping threshold for the model parameterized in Table 3. The NCT is averaged over 10^4 simulation runs. It shows that the average computational complexity can be reduced by more than 40% when a 25 dB clipping threshold is adopted for the "Indoor LOS" case, while a 15% improvement can be expected for the "Outdoor NLOS" case if $P_{th} = 15$ dB. The NLOS case requires a higher clipping threshold with respect to the LOS case to archive the same NCT reduction. As for the LOS case, the power of LOS ray is stronger than the NLOS rays such that most clusters were clipped out for a low threshold. For the NLOS case, the power difference among clusters is not so large as for the LOS case. So, even with a lower threshold, clusters are more likely to be clipped.

To keep the total power of the remaining clusters unitary, the loss of the power of the clipped clusters needs to be compensated. For a given threshold, P_{th}, the indexing set $\mathcal{I}$ can be separated into two disjoint sets, $\mathcal{I}_0 = \{n : P_n < \max_{k\in\mathcal{I}} P_k - P_{th}\}$ and its complement $\mathcal{I}_1 = \mathcal{I} \setminus \mathcal{I}_0$. If cluster n is clipped subject to a certain threshold, its power, P_n, can be combined with the power of the closest neighboring cluster m which is given by

$$m = \arg\min_{k\in\mathcal{I}_1} |\tau_k - \tau_n|, \quad \forall n \in \mathcal{I}_0. \tag{12}$$

A direct consequence of clipping clusters is the bias in the RMS delay spread which is inversely proportional to the coherent bandwidth, a critical parameter. For a given drop, denotes the RMS delay spread before and after clipping with a threshold P_{th} as τ_{RMS} and $\widetilde{\tau}_{\text{RMS}}$, respectively. The mean relative error (MRE) of the RMS delay spread versus the clipping threshold is defined by

$$\epsilon_{\text{DS}}(P_{\text{th}}) = \text{E}\left(\frac{\left|\widetilde{\tau}_{\text{RMS}} - \tau_{\text{RMS}}\right|}{\tau_{\text{RMS}}}\right), \tag{13}$$

which is plotted in Figure 2(b). It shows, as expected, that as the threshold becomes larger, the relative error ϵ_{DS} becomes smaller. The MRE of DS is more sensitive to the clipping threshold in the NLOS case. Particularly, ϵ_{DS} is around 5% when the clipping threshold $P_{\text{th}} = 15\,\text{dB}$ for the outdoor NLOS case or $P_{\text{th}} = 25\,\text{dB}$ for the indoor LOS case.

4.2. Fixed RMS Delay Spread. In order to estimate a given performance metric via Monte Carlo simulation, the number of random samples required to achieve a given level of confidence depends on the number of RVs involved in the simulation. As mentioned above, random realizations of five LSPs need to be drawn from their own distributions. The angular spread at both ends of the link, that is, ASD and ASA, will have a crucial impact on the spatial correlation properties of the MIMO channel. Hence, we propose fixing the RMS DS at its mean value to reduce the number of RVs. Although this will change the per drop behavior of the channel model, mainly in the delay domain, the average behavior will only be slightly affected as shown in Section 5.

4.3. Fixed XPR. In addition to fixing the RMS DS as a constant, we can also fix the XPR. The behavior of MIMO systems with cross-polarized antennas was investigated in [27] with the 3GPP/3GPP2 SCM model. These results showed that the change in mean capacity as the XPR varies is negligible for a $\pm 45^{\circ}$ cross-polarized 2×2 system. Hence, we propose fixing the XPR at its mean value and investigate the impact of this simplification on the metrics given in Section 3.

4.4. Uncorrelated LSPs. The LSPs, DS, ASD, ASA, SF, and Rician-K factor, are correlated in the baseline channel model. However, as shown in Table 3, the parameters extracted from field measurements show that some LSPs are weakly correlated or even uncorrelated, for example, Rician-K factor versus ASA or ASD, ASD versus ASA, DS versus ASA, and so forth. Some similar weak correlation properties are also reported in the literature [16, 17]. We remove the correlations between the LSPs and investigate the impact of this simplification.

5. Results and Discussions

5.1. Channel Measurements and Parameter Extraction

5.1.1. Measurement System. To extract the parameters required by the baseline model, wideband channel data were collected using the Elektrobit Propsound CS [28] MIMO channel sounder, which uses pseudorandom binary signals (PRBS) and time-division multiplexed (TDM) switching. The transmitted power was 26 dBm and the length of the PRBS was 511 symbols. The transmitter (TX) was equipped with a dual-polarized omnidirectional array (ODA) with a maximum of 50 elements. The receiver (RX) employed a vertically polarized 8-element uniform circular array (UCA). Figures 3(a) and 3(b) show, respectively, the configurations of the TX and RX antenna arrays. Schematic plots of both antenna arrays are given in Figure 4. The spacing between the neighboring elements in both the ODA and the UCA is half a wavelength. All 8×50 subchannels are sounded by activating each TX-RX element pair consecutively within a time period which is referred to as a measurement cycle. A temporal snapshot refers to the impulse response measured within a measurement cycle. The temporal snapshot rate is also the cycle rate. The measurement settings are summarized in Table 2.

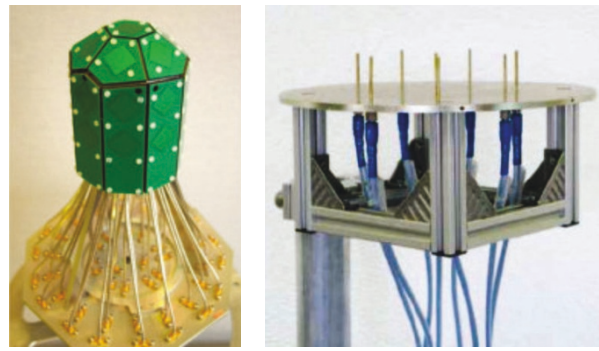

(a) TX array (b) RX array

Figure 3: Configurations of the antenna arrays used in the measurements.

Table 2: General sounder parameters.

Item	Setting
Center frequency	5.25 GHz
Chip rate	100 MHz
Sampling rate	200 MHz
TX power at antenna input	26 dBm
PN code length	511
Temporal snapshot rate	21.7 Hz
Number of elements of TX array	50
Number of elements of RX array	8

5.1.2. Measurement Environment. Stationary measurements were conducted in the corridor of a teaching building on the campus of Beijing University of Posts and Telecommunications (BUPT), China as the indoor scenario [29]. The dimension of a single floor is $120 \times 45 \times 6\,\text{m}^3$. The TX array and RX array were located about 1.5 m and 2.5 m above the floor level, respectively. All 8×50 elements on both TX and RX arrays are enabled during the measurements.

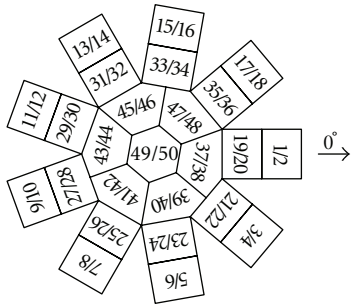

(a) TX array

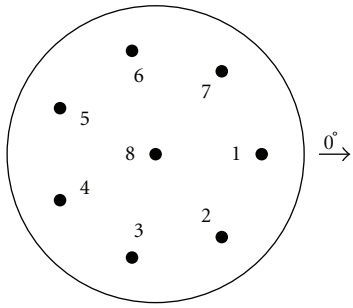

(b) RX array

Figure 4: Schematic plots of the antenna arrays used in the measurements.

Figure 5 illustrates the layout of indoor measurements in the corridor. The RX was fixed as the base station and is marked with the arrow denoting the reference direction. The TX was measured at the 32 locations marked as "TX Position." At each spot, 100 temporal snapshots of raw data were recorded. In this environment, the walls along the corridor and between the rooms are made of bricks with plastic poster boards on the surface. The floor has a marble surface and the doors of the rooms are wooden. The entrance doors are made of glass with aluminum frames.

5.1.3. Method of Noise Cut. Receiver noise was superimposed on the measured CIRs. Hence, before either estimating channel parameters or determining capacity in (5), we need to choose an appropriate dynamic range of the measured CIRs to perform the noise cut. Following [30], the *per subchannel dynamic noise cut* method is applied in this paper. Given a temporal snapshot, the noise floor P_{floor} was calculated for each subchannel. As a rule of thumb, a 6 dB noise margin Δ_{noise} added to the estimated noise floor can guarantee the noise is better cut. The per subchannel dynamic range of a measured CIR is defined as

$$\mathrm{DR} = \min\left\{P_{\text{peak}} - \left(P_{\text{floor}} + \Delta_{\text{noise}}\right), \mathrm{DR}_{\max}\right\}, \tag{14}$$

where P_{peak} is the peak value of PDP for the given subchannel and $\mathrm{DR}_{\max} = 25$ dB is the predefined maximum dynamic range.

5.1.4. Parameters for the Baseline Model. For each temporal snapshot, the multipath channel is described by the superposition of L rays. The rays are characterized by the parameter

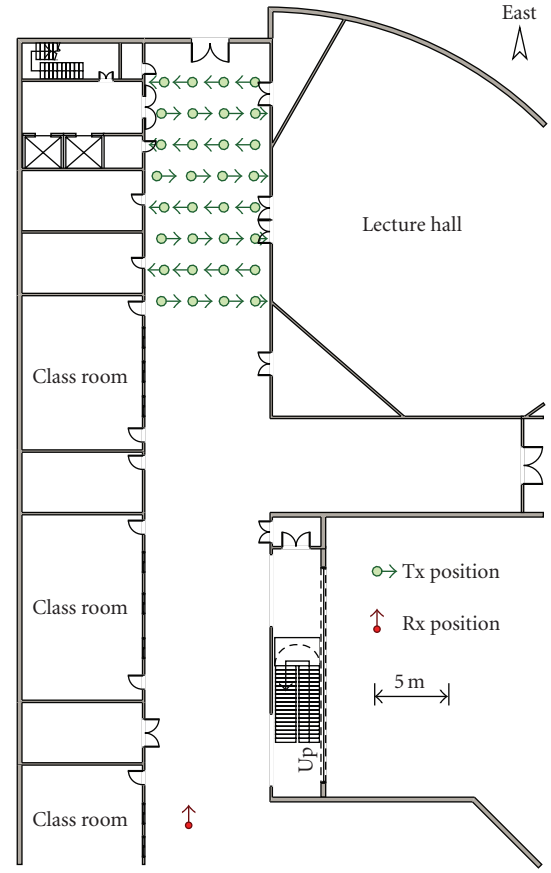

Figure 5: Layout of the indoor measurements in the corridor.

set $\mathcal{P} = \{(\tau_\ell, \phi_\ell, \theta_\ell, \varphi_\ell, \vartheta_\ell, \nu_\ell, \mathbf{X}_\ell) : \ell = 1, 2, \ldots, L\}$. Here, τ_ℓ, ϕ_ℓ, θ_ℓ, φ_ℓ, ϑ_ℓ, and ν_ℓ denote the excess delay, the azimuth of departure, the elevation of departure, the azimuth of arrival, the elevation of arrival, and the Doppler shift of the ℓth ray. The polarization matrix reads $\mathbf{X}_\ell = (\alpha_{\ell,p_2,p_1})_{2\times 2}$. The complex entry α_{ℓ,p_2,p_1} represents the weight for the ℓth ray that originates in the p_1 direction and arrives in the p_2 direction. Under the assumption of far-field and planar wave propagation, the Space-Alternating Generalized Expectation maximization (SAGE) algorithm [31, 32] is utilized to estimate the parameter set $\mathcal{P}$ from each temporal snapshot of the measured CIRs. The first- and second-order statistics of these parameters in $\mathcal{P}$ correspond to the LSPs described in Section 2, and are summarized in Table 3. The estimated maximum Doppler shift f_{D} is 1 Hz for the indoor measurements.

For reasons of space a full description of the parameter extraction methodology cannot be given here. However, the references [16, 31, 32] contain the necessary details. The basic approach can be summarized as below. The measured data is taken and the SAGE algorithm [31, 32] is used to obtain samples of the 7 parameters in $\mathcal{P}$ from each temporal snapshot. Following the WINNER methodology [16], these samples are then used to find the parameters in the columns entitled "Indoor" in Table 3. Finally, these tabulated parameters are sufficient to define the terms in

Table 3: Parameters for the baseline channel model.

Parameter	Unit	Indoor[a]	Outdoor[b]	Parameter	Unit	Indoor[a]	Outdoor[b]
μ_{DS}	$\log_{10}[s]$	−7.70	−7.12	$\rho_{ASD,DS}$		0.17	0.20
σ_{DS}		0.18	0.12	$\rho_{ASA,DS}$		0.01	0.40
μ_{ASD}	$\log_{10}[^\circ]$	1.60	1.19	$\rho_{ASA,SF}$		−0.02	−0.40
σ_{ASD}		0.18	0.21	$\rho_{ASD,SF}$		−0.18	0.00
μ_{ASA}		1.62	1.55	$\rho_{DS,SF}$		−0.18	−0.70
σ_{ASA}		0.22	0.20	$\rho_{ASD,ASA}$		0.07	0.10
σ_{SF}	dB	3.0	4.0	$\rho_{ASD,K}$	—	−0.09	N/A
μ_K		4.7	N/A	$\rho_{ASA,K}$		−0.07	N/A
σ_K		0.9	N/A	$\rho_{DS,K}$		−0.32	N/A
r_τ	—	3.6	1.0	$\rho_{SF,K}$		0.57	N/A
μ_{XPR}	dB	3.7	8.0	Cluster ASD	°	5	10
σ_{XPR}		9.6	3.0	Cluster ASA		11	22
N	—	15	16	M	—	20	20

[a]Parameters for the indoor case are obtained from the measurements described in Section 5.1.
[b]The NLOS case of the "Urban macrocell (C2)" scenario in the WINNER channel model [16].

the channel coefficients given in (2) and (3) by the steps described in [16].

Besides the indoor LOS case, an outdoor NLOS case is also selected as shown in Table 3. The parameters in the columns entitled "Outdoor" are the same as those for the NLOS case of the "Urban macrocell (C2)" scenario in the WINNER channel model [16]. The definition of each parameter can be found in Section 2.

5.2. Simulation Assumptions. To investigate the impact of the proposed simplifications on channel behavior, we constrain the antenna configuration and bandwidth to match the measurement campaign. We select 9 elements from the 50-element MS array and 7 elements from the 8-element BS array to form a 9×7 downlink MIMO channel. This approach is both manageable from a complexity point of view and is in agreement with the measurement configuration described previously. The selected BS array is a 7-element vertical polarized uniform circular array, that is, the 7+1 UCA without the central element. The MS antenna array is a 9-element dual-polarized uniform circular array which can be thought as the center ring of the 2×9 ODA (with odd elements from no. 19 to no. 35 in Figure 4(a)). For both antenna arrays, the element spacing is half a wavelength. The field patterns of real antennas are embedded into the baseline and simplified models to regenerate equivalent sets of MIMO channel matrix realizations. The embedding of field patterns is archived by substitution of the array patterns obtained in an anechoic chamber as $\mathbf{c}_{BS,s}$ and $\mathbf{c}_{MS,u}$ into (2) and (3). The channel coefficients are generated following [33] and by replacing the scenario specific parameters in [33] with those in Table 3. For the indoor case, all other parameters of the model are set to match those obtained in the measurement campaign. This includes reference directions for both antenna arrays. The assumptions are summarized in Table 4. The channel is sampled at a frequency four times the maximum Doppler frequency. The results are obtained by averaging over 1000 simulation runs(or drops) [14]. (The number of drops is chosen to be manageable from a complexity point of view and also to ensure satisfactory convergence of the metric.) The fading distance of 50 wavelengths is assumed for each drop.

For brevity, we designate the simplified models as "SM-" suffixed with a letter. SM-A refers to the full model where the clusters are clipped out with a 25 dB threshold for the indoor LOS case or a 15 dB threshold for the outdoor NLOS case. SM-B takes the full model and fixes RMS DS as a constant. SM-C fixes XPR at its mean value and SM-D removes the cross-correlations between LSPs. SM-E applies all the simplifications in SM-A, B, C, and D simultaneously. The designators are listed in Table 5. In the following simulation results, the measured results are given as a reference for Indoor scenario only.

5.3. Simulation Results and Discussion

5.3.1. Ordered Eigenvalue Distributions. The marginal CDFs of the first five principal eigenvalues for the baseline and simplified models are as shown in Figure 6. It can be seen that the proposed simplifications have a very minor impact on the distribution of the first principal eigenvalue. Removing the cross-correlations between LSPs has made little change to the distribution of ordered eigenvalues. Similarly, fixing the RMS DS leads to a negligible effect on the eigenvalues. As predicted, the impact on the spatial correlations is not significant and hence there is little impact on the eigenvalues. Figure 6(a) also tells us that the distortion of different ordered eigenvalues differs when SM-C or SM-E is applied. For example, with SM-C, $\lambda_{(2)}$ is underestimated while $\lambda_{(4)}$ and $\lambda_{(5)}$ are overestimated with respect to the baseline model. Figure 6(b) shows that for outdoor NLOS case, the ordered eigenvalue distribution is less sensitive to all simplifications.

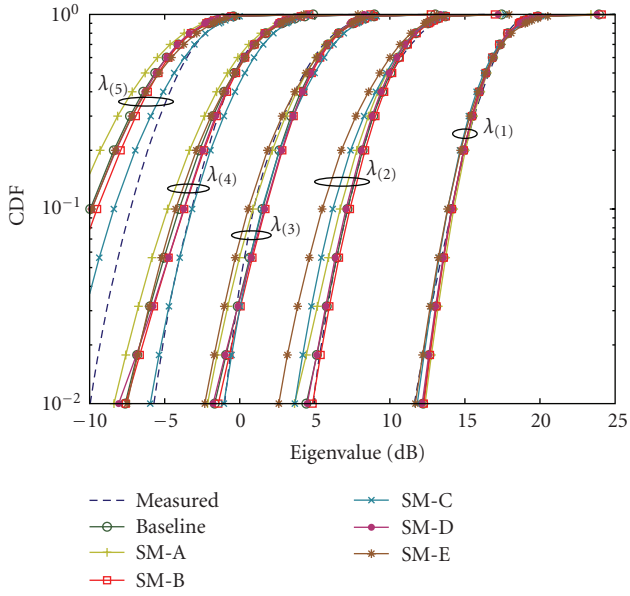

(a) Indoor LOS case

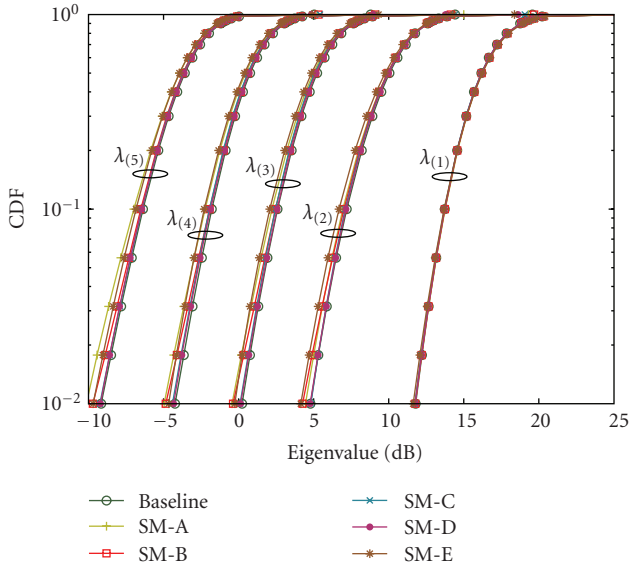

(b) Outdoor NLOS case

Figure 6: CDFs of the first five principal eigenvalues for baseline and simplified cases.

Note that in the measurement-based indoor baseline model, the nonprincipal eigenvalues deviate from the measured results. The relative deviation of the eigenvalue becomes larger for smaller eigenvalues.

5.3.2. Outage Capacity. Broadband capacity are obtained by integrating the narrowband capacity over the entire bandwidth as in (5). The CDFs of MIMO capacity for the baseline and simplified models are depicted in Figure 7. There are three different SNR levels which represent the marginal, medium, and high SNR cases. We see that the baseline and simplified models always underestimate the MIMO capacity

Table 4: Assumptions of channel reconstruction.

Parameter	Description
Carrier frequency	5.25 GHz
Bandwidth	100 MHz
BS antenna array	7-element UCA, vertical polarized
MS antenna array	9-element UCA, $\pm 45^\circ$ dual polarized
MS velocity	1.5 km/h (indoor) and 120 km/h (outdoor)
Sample density	2 samples per half wavelength
No. of drops	1000
No. of time samples per drop	200
Delay sampling density	5 ns
No. of frequency bins	1024

with respect to the measured result. This underestimation comes from several aspects such as measurement errors and possibly the lack of elevation spread in the models, which was theoretically analyzed in [34]. For the indoor LOS case, the variations in MIMO capacity due to the proposed simplifications increase as the SNR increases. With SM-E, the relative deviation of the capacity for an outage of 5% at high SNR ($\rho = 20$ dB) is 4.23%. Since the use of SM-E will lead to the maximum deviation in outage capacity, the relative deviation of the capacity for outages of 5% due to the application of any proposed simplified model will not exceed 5% in the high SNR regime. For the outdoor NLOS case, the relative deviation is always less than 5%.

As shown in Figure 7(a), there is a deviation of the baseline model from the measurements in the high SNR case. This deviation is mainly caused by the deviation of nonprincipal eigenvalues. For a given frequency f, denote the measured and model generated $U \times S$ channel matrix as $\mathbf{H}(f)$ and $\mathbf{H}'(f)$, respectively. Let $\lambda_{(n)}$ and $\lambda'_{(n)}$ be the ordered eigenvalues of $\mathbf{H}(f)\mathbf{H}(f)^\dagger$ and $\mathbf{H}'(f)\mathbf{H}'(f)^\dagger$, respectively, where $\lambda_{(1)} \geqslant \lambda_{(2)} \geqslant \cdots \geqslant \lambda_{(U)}$ and $\lambda'_{(1)} \geqslant \lambda'_{(2)} \geqslant \cdots \geqslant \lambda'_{(U)}$. Assume the eigenvalues can be divided into two sets: the well fitted principal eigenvalues in $\mathcal{L}_1 = \{(\lambda_{(n)}, \lambda'_{(n)}) : n = 1, 2, \ldots, r'\}$ with negligible relative deviation; and small eigenvalues in $\mathcal{L}_2 = \{(\lambda_{(n)}, \lambda'_{(n)}) : n = r'+1, r'+2, \ldots, U\}$ with large deviations. When the SNR $\rho \to \infty$, the capacity deviation tends to

$$\begin{aligned} \epsilon_C &= \lim_{\rho \to \infty} \sum_{n=1}^{U} \log_2 \frac{1 + (\rho/S)\lambda'_{(n)}}{1 + (\rho/S)\lambda_{(n)}} \\ &= \sum_{n=1}^{r'} \log_2 \left(1 + \frac{\Delta\lambda_{(n)}}{\lambda_{(n)}}\right) + \sum_{n=r'+1}^{U} \log_2 \left(1 + \frac{\Delta\lambda_{(n)}}{\lambda_{(n)}}\right), \end{aligned} \tag{15}$$

where $\Delta\lambda_{(n)} = \lambda'_{(n)} - \lambda_{(n)}$. The first term in (15) approximates to zero as the relative deviation $\Delta\lambda_{(n)}/\lambda_{(n)}$ is very small. For the eigenvalues in $\mathcal{L}_2$, the nonnegligible relative deviation $\Delta\lambda_{(n)}/\lambda_{(n)}$ causes the capacity deviation. In Figure 6(a), we can take $r' = 4$. For the probability of 0.5, we have $\lambda_{(5)} = -4.0$ dB $= 0.40$ and $\lambda'_{(5)} = -5.6$ dB $= 0.28$. Thus, $\Delta\lambda_{(5)}/\lambda_{(5)} = -0.43$, and $\log_2(1+\Delta\lambda_{(n)}/\lambda_{(n)}) = -0.81$ bit/s/Hz.

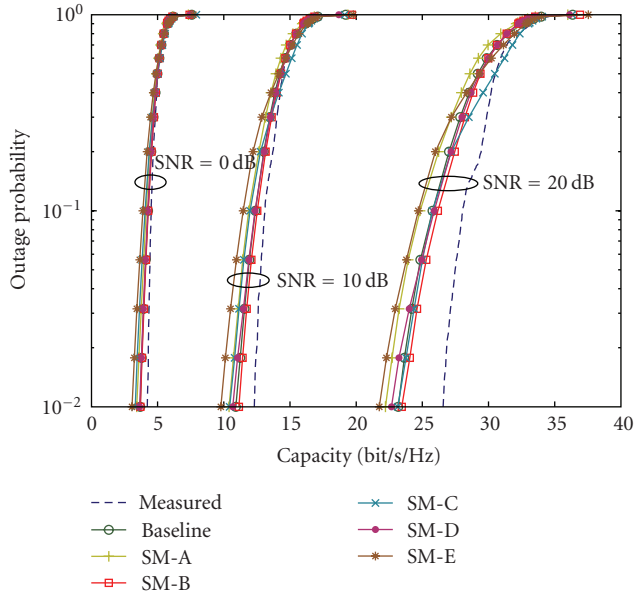

(a) Indoor LOS case

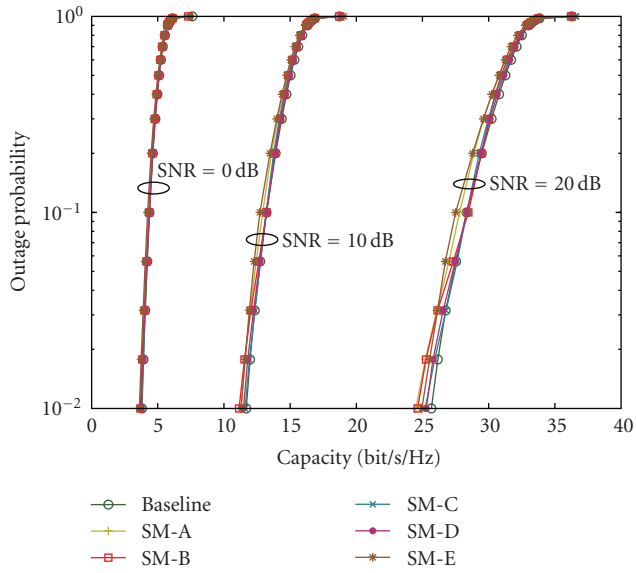

(b) Outdoor NLOS case

Figure 7: CDFs of MIMO capacity for baseline and simplified cases.

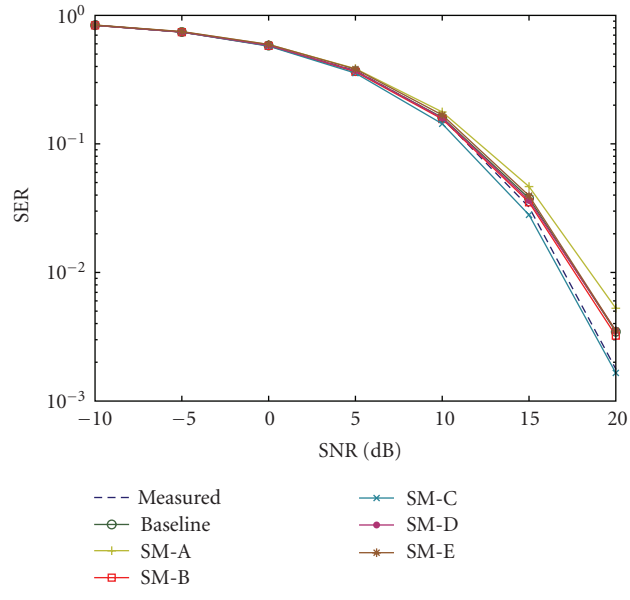

(a) Indoor LOS case

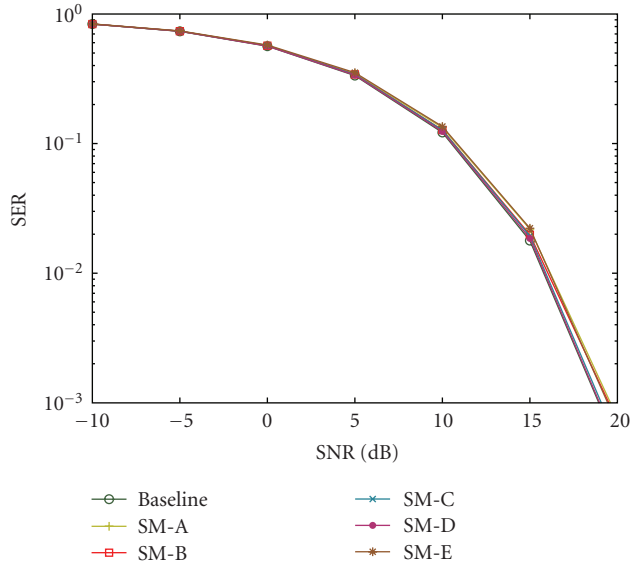

(b) Outdoor NLOS case

Figure 8: SVD symbol error probabilities for baseline and simplified cases.

For $n = 6$ and $n = 7$, larger deviations of eigenvalues can be expected, which finally lead to the gap between the measurements and the baseline model as shown in Figure 7(a).

5.3.3. Symbol Error Probability. For the indoor case, consider the baseline model extracted from the measurements conducted in the LOS environment. The gain of the last three MIMO eigenmodes is limited due to the presence of the LOS ray. Consequently, we consider the SVD transmission over the first four principal eigenmodes. The symbol error rates for the baseline and simplified models are shown in Figure 8(a). In the low SNR regime, all simplified models perform almost identically to the baseline model. However, in the high SNR regime, there is an approximate shift of 1 dB in SNR for an SER of 10^{-2} due to both SM-A and SM-C

Table 5: Designators for simplified models.

Designator	Simplification
SM-A	Clip out clusters with a 25 dB (for indoor LOS case) or 15 dB (for outdoor NLOS case) threshold.
SM-B	Fix the RMS DS as the mean value μ_{DS} in Table 3.
SM-C	Fix the XPR as the mean value μ_{XPR} in Table 3.
SM-D	Remove cross-correlations between all LSPs.
SM-E	All simplifications in SM-A, SM-B, SM-C, and SM-D.

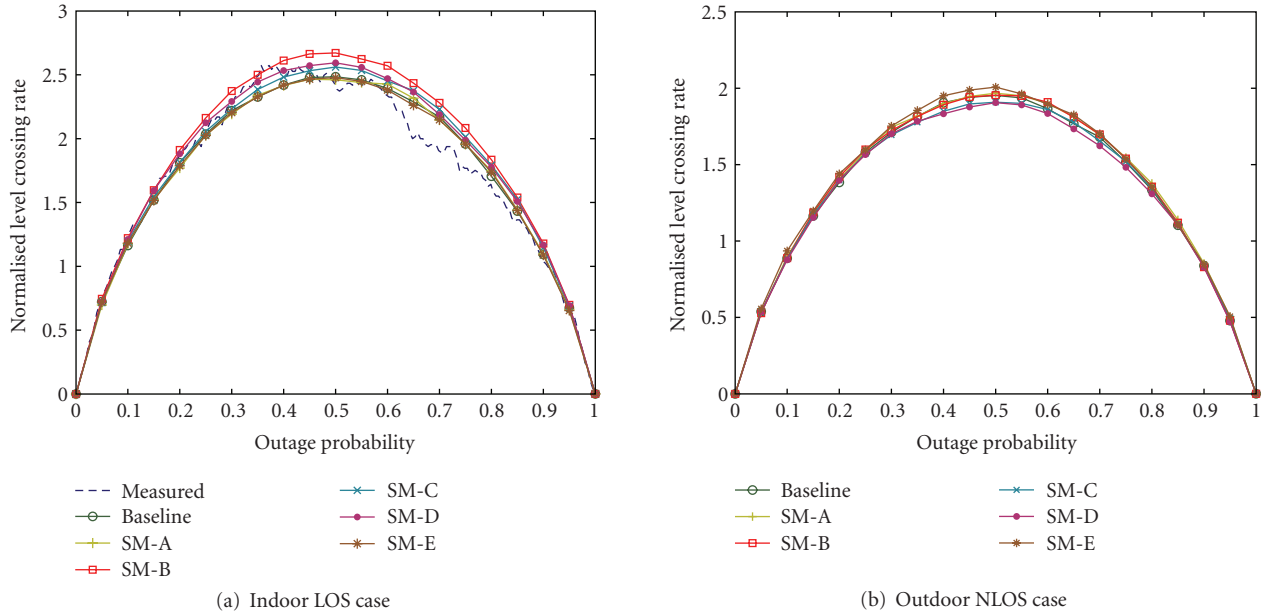

(a) Indoor LOS case (b) Outdoor NLOS case

Figure 9: Level crossing rates of standardized MIMO capacity for baseline and simplified cases when $\rho = 20$ dB.

Table 6: Comparisons between the baseline model and SM-E model.

Item		Indoor LOS		Outdoor NLOS	
		Baseline	SM-E	Baseline	SM-E
Complexity	No. of parameters	26	14	20	12
	No. of RVs	6	4	5	3
	NCT per drop	100%	57%	100%	85%
Accuracy	Relative deviation of $C_{5\%}$	0	<5%	0	<5%
	SNR shift for SER of 10^{-2}	0	<1 dB	0	<0.5 dB
	LCR for outage below 10%	Approximately equal			

for the indoor LOS case. Again, the performance variation due to both SM-B and SM-D is negligible. It is worth noting that the performance of SM-E is nearly the same as the baseline model across the whole SNR range. Although conventional wisdom says that large delays will result in higher error rates due to frequency-selective fading. However according to (8), the frequency-selective channel is effectively decomposed into a series of flat-fading channels, hence the SER result here does not show any sensitivity to the delay randomness. The symbol error rates for the outdoor case are plotted in Figure 8(b) which shows negligible deviations of all simplified models from the baseline model.

5.3.4. LCR for the Standardized MIMO Capacity. The normalized LCR of standardized MIMO capacity at 20 dB SNR is given in Figure 9 which shows that all simplified models cross-capacity thresholds for outage levels below 10% at nearly same rate. It means that all simplified models exhibit a similar temporal behavior for MIMO capacity as the baseline model for both indoor- and outdoor cases.

5.3.5. Comparisons. We compare the baseline model and the simplified model, SM-E, from an accuracy and complexity point of view in Table 6. The complexity of a channel model is two fold: (a) the time for generating channel coefficients; and (b) the time for convolution of the transmitted signal and the channel [26]. Since the real computational time depends on many factors such as the implementation of the model and the computational power of the simulation platform, we employ some indirect metrics and evaluate the complexity. The number of parameters used is related to the time of coefficient generation and is referred to as the number of parameters required to describe a model. For the baseline model, it equals the number of items listed in Table 3, that is, 26 for the indoor LOS scenario and 20 for the outdoor NLOS scenario. For SM-E, the following parameters are not required: σ_{DS}, σ_{XPR}, and 10 (for LOS) or 6 (for NLOS) cross-correlation coefficients. Hence, only 14 or 12 parameters are required to describe the SM-E model. The number of RVs is another value of interest, since the metrics of interest in simulation (e.g., bit error rate) require less time to converge when the number of RVs in the model is reduced. For the baseline model, there are 6 (for LOS) or 5 (for NLOS) RVs, that is, 5 (for LOS) or 4 (for NLOS) random LSPs and the random XPR. With SM-E, both DS and XPR are fixed as constants and only 4 or 3 RVs remain. Recall that the NCT measure can reflect the convolution reduction. The NCT is

obtained by approximating (11) through simulation. The results show that the SM-E is an acceptable tradeoff between accuracy and complexity with respect to the baseline model.

6. Conclusion

In this paper, we have studied the simplification of the GBSM by several approaches. The double-directional channel model developed under the IST-WINNER project is employed as the baseline model. The parameters for the indoor LOS baseline model are extracted by applying the SAGE algorithm to the data obtained from channel measurements. Four metrics are proposed to evaluate the impact of the simplifications on the behavior of the channel models. These include the MIMO capacity, eigenvalue distributions, symbol error rate of SVD-transmission, and level crossing rate of the MIMO capacity. Five different simplified models are developed based on the baseline model with the following modifications:

(i) SM-A: clipping clusters with a 25 dB (for indoor LOS case) or 15 dB (for outdoor NLOS case) power threshold,

(ii) SM-B: fixing the RMS DS at its mean value,

(iii) SM-C: fixing the XPR at its mean value,

(iv) SM-D: removing cross-correlations between LSPs,

(v) SM-E: all the above modifications.

The simulation results show that all these five simplified models have a minor impact on all proposed metrics. Compared to the baseline model, the SM-E can provide much better computational efficiency with a negligible loss of accuracy. Besides the two scenarios presented in this paper, we have repeated the simulations for all other scenarios in the WINNER model. All these simulation results support our conclusion. However, for reasons of space we cannot present those results in this paper. This means that fixed parameters and fewer random parameters can be used to give similar results. We have shown that simplification is possible and perhaps further simplifications might follow to make the models even more appealing. The simplified models have been far more rigorously tested. Instead of only looking at spatial and temporal correlations, we have looked at full system behavior in terms of many metrics. Furthermore, since the simplifications keep the original structure of the GBSM, the antenna geometries and radiation patterns can still be changed by the users as these parameters remain part of the simplified model. We also find that the baseline model underestimates the outage capacity with respect to the measurements. This might be due to measurement errors, modeling errors of nonprincipal eigenvalues or possibly the neglect of angular spread in elevation. Hence, simplifications of three-dimensional GBSMs will be considered in future work.

Acknowledgments

The authors would like to thank the engineers of Elektrobit Testing Ltd., Finland, for their efforts in the measurement campaign. Discussions with Doctor Guangyi Liu and Weihui Dong from China Mobile have been enlightening. They also appreciate the useful comments from the anonymous reviewers. This work was supported in part by the National 863 High Technology Research and Development Program of China under Grant No. 2006AA01Z258, and by the Research Institute of China Mobile Communications Corporation.

References

[1] J. H. Winters, "On the capacity of radio communication systems with diversity in a Rayleigh fading environment," *IEEE Journal on Selected Areas in Communications*, vol. 5, no. 5, pp. 871–878, 1987.

[2] E. Telatar, "Capacity of multi-antenna Gaussian channels," *European Transactions on Telecommunications*, vol. 10, no. 6, pp. 585–595, 1999.

[3] G. J. Foschini and M. J. Gans, "On limits of wireless communications in a fading environment when using multiple antennas," *Wireless Personal Communications*, vol. 6, no. 3, pp. 311–335, 1998.

[4] P. Kyritsi, D. C. Cox, R. A. Valenzuela, and P. W. Wolniansky, "Effect of antenna polarization on the capacity of a multiple element system in an indoor environment," *IEEE Journal on Selected Areas in Communications*, vol. 20, no. 6, pp. 1227–1239, 2002.

[5] C. Oestges and B. Clerckx, "Modeling outdoor macrocellular clusters based on 1.9-GHz experimental data," *IEEE Transactions on Vehicular Technology*, vol. 56, no. 5, pp. 2821–2830, 2007.

[6] J. W. Wallace, M. A. Jensen, A. Gummalla, and H. B. Lee, "Experimental characterization of the outdoor MIMO wireless channel temporal variation," *IEEE Transactions on Vehicular Technology*, vol. 56, no. 3, pp. 1041–1049, 2007.

[7] M. Landmann, K. Sivasondhivat, J.-I. Takada, I. Ida, and R. Thomä, "Polarization behavior of discrete multipath and diffuse scattering in urban environments at 4.5 GHz," *EURASIP Journal on Wireless Communications and Networking*, vol. 2007, Article ID 57980, 16 pages, 2007.

[8] S. Wyne, A. F. Molisch, P. Almers, G. Eriksson, J. Karedal, and F. Tufvesson, "Outdoor-to-indoor office MIMO measurements and analysis at 5.2 GHz," *IEEE Transactions on Vehicular Technology*, vol. 57, no. 3, pp. 1374–1386, 2008.

[9] P. Almers, E. Bonek, A. Burr, et al., "Survey of channel and radio propagation models for wireless MIMO systems," *EURASIP Journal on Wireless Communications and Networking*, vol. 2007, Article ID 19070, 19 pages, 2007.

[10] D.-S. Shiu, G. J. Foschini, M. J. Gans, and J. M. Kahn, "Fading correlation and its effect on the capacity of multielement antenna systems," *IEEE Transactions on Communications*, vol. 48, no. 3, pp. 502–513, 2000.

[11] W. Weichselberger, M. Herdin, H. Özcelik, and E. Bonek, "A stochastic MIMO channel model with joint correlation of both link ends," *IEEE Transactions on Wireless Communications*, vol. 5, no. 1, pp. 90–100, 2006.

[12] L. M. Correia, Ed., *Wireless Flexible Personalised Communications: COST 259, European Co-Operation in Mobile Radio Research*, John Wiley & Sons, Chichester, UK, 2001.

[13] L. M. Correia, Ed., *Mobile Broadband Multimedia Networks: Techniques, Models and Tools for 4 G*, Academic Press, Oxford, UK, 2006.

[14] G. Calcev, D. Chizhik, B. Göransson, et al., "A wideband spatial channel model for system-wide simulations," *IEEE*

Transactions on Vehicular Technology, vol. 56, no. 2, pp. 389–403, 2007.

[15] "IST-2003-507581 WINNER D5.4 v1.4 Final report on link level and system level channel models," November 2005, http://www.ist-winner.org/DeliverableDocuments/D5.4.pdf.

[16] "IST-4-027756 WINNER II D1.1.2 v1.2 WINNER II channel models," February 2008, http://www.ist-winner.org/WINNER2-Deliverables/D1.1.2.zip.

[17] "Working document towards proposed draft new report [Guidelines for evaluation of radio interface technologies for IMT-Advanced]," ITU-R Document 5D/TEMP/90-E, International Telecommunication Union (ITU), Geneva, Switzerland, June 2008.

[18] M. Failli, Ed., *COST 207: Digital Land Mobile Radio Communications, Final Report*, European Commission, Luxembourg, Belgium, 1989.

[19] "Guidelines for evaluation of radio transmission technologies for IMT-2000," ITU-R Recommendation M.1225, International Telecommunication Union (ITU), Geneva, Switzerland, February 1997.

[20] P. J. Smith and M. Shafi, "The impact of complexity in MIMO channel models," in *Proceedings of IEEE International Conference on Communications (ICC '04)*, vol. 5, pp. 2924–2928, Paris, France, June 2004.

[21] A. Forenza, D. J. Love, and R. W. Heath Jr., "Simplified spatial correlation models for clustered MIMO channels with different array configurations," *IEEE Transactions on Vehicular Technology*, vol. 56, no. 4, part 2, pp. 1924–1934, 2007.

[22] H. Asplund, J. Medbo, B. Göransson, J. Karlsson, and J. Sköld, "A simplified approach to applying the 3GPP spatial channel model," in *Proceedings of the 17th IEEE International Symposium on Personal, Indoor and Mobile Radio Communications (PIMRC '06)*, pp. 1–5, Helsinki, Finland, September 2006.

[23] A. F. Molisch, M. Steinbauer, M. Toeltsch, E. Bonek, and R. S. Thomä, "Capacity of MIMO systems based on measured wireless channels," *IEEE Journal on Selected Areas in Communications*, vol. 20, no. 3, pp. 561–569, 2002.

[24] L. M. Garth, P. J. Smith, and M. Shaft, "Exact symbol error probabilities for SVD transmission of BPSK data over fading channels," in *Proceedings of IEEE International Conference on Communications (ICC '05)*, vol. 4, pp. 2271–2276, Seoul, South Korea, May 2005.

[25] A. Giorgetti, P. J. Smith, M. Shafi, and M. Chiani, "MIMO capacity, level crossing rates and fades: the impact of spatial/temporal channel correlation," *Journal of Communications and Networks*, vol. 5, no. 2, pp. 104–115, 2003.

[26] P. Kyösti and T. Jämsä, "Complexity comparison of MIMO channel modelling methods," in *Proceedings of the 4th IEEE Internatilonal Symposium on Wireless Communication Systems (ISWCS '07)*, pp. 219–223, Trondheim, Norway, October 2006.

[27] P. J. Smith and M. Shafi, "The use of cross-polarized antennas for MIMO systems," in *Proceedings of the Australian Communications Theory Workshop (AusCTW '04)*, Newcastle, Australia, February 2004.

[28] Elektrobit Corporation, "EB Propsound CS: radio channel measurement and research," 2008, http://www.elektrobit.com/index.php?209.

[29] X. Gao, J. Zhang, G. Liu, et al., "Large-scale characteristics of 5.25 GHz based on wideband MIMO channel measurements," *IEEE Antennas and Wireless Propagation Letters*, vol. 6, pp. 263–266, 2007.

[30] X. Zhao, J. Meinilä, L. Hentilä, T. Jämsä, P. Kyösti, and J.-P. Nuutinen, "Effects of noise cut for extraction of wideband channel parameters," in *Proceedings of the 18th IEEE International Symposium on Personal, Indoor and Mobile Radio Communications (PIMRC '07)*, pp. 1–4, Athens, Greece, September 2007.

[31] B. H. Fleury, M. Tschudin, R. Heddergott, D. Dahlhaus, and K. I. Pedersen, "Channel parameter estimation in mobile radio environments using the SAGE algorithm," *IEEE Journal on Selected Areas in Communications*, vol. 17, no. 3, pp. 434–450, 1999.

[32] X. Yin, B. H. Fleury, P. Jourdan, and A. Stucki, "Polarization estimation of individual propagation paths using the SAGE algorithm," in *Proceedings of the 14th International Symposium on Personal, Indoor and Mobile Radio Communications (PIMRC '03)*, vol. 2, pp. 1795–1799, Beijing, China, Sepember 2003.

[33] L. Hentilä, P. Kyösti, M. Käske, M. Narandzic, and M. Alatossava, "MATLAB implementation of the WINNER Phase II Channel Model ver1.1," December 2007, http://www.ist-winner.org/phase_2_model.html.

[34] M. Shafi, M. Zhang, P. J. Smith, A. L. Moustakas, and A. F. Molisch, "The impact of elevation angle on MIMO capacity," in *Proceedings of IEEE International Conference on Communications (ICC '06)*, vol. 9, pp. 4155–4160, Istanbul, Turkey, June 2006.